Springer

KSME

Journal of Mechanical Science and Technology 26 (1) (2012) 161~172
www.springerlink.com/content/1738-494x
DOI 10.1007/s12206-011-1022-7

A cross-sectional analysis of composite beams based on asymptotic framework †

Joonho Jeong[1], Jun-Sik Kim[2], Yeon June Kang[3] and Maenghyo Cho[4,*]

[1]*Interdisciplinary Program in Automotive Engineering, Seoul National University, Seoul, 151-742, Korea*
[2]*Department of Intelligent Mechanical Engineering, Kumoh National Institute of Technology, Gumi, Gyeongbuk, 730-701, Korea*
[3]*School of Mechanical and Aerospace Engineering, Seoul National University, Seoul, 151-742, Korea*
[4]*WCU Multiscale Mechanical Design Division, School of Mechanical and Aerospace Engineering, Seoul National University, Seoul, 151-742, Korea*

(Manuscript Received May 11, 2011; Revised September 26, 2011; Accepted October 5, 2011)

Abstract

This paper presents the accurate prediction of static behavior of composite beams with arbitrary cross-sections. The asymptotic recursive formulation is reviewed first, where the initial three-dimensional problems are split into the macroscopic 1D problems and the microscopic 2D problems. The finite element formulation for the microscopic 2D problems is then presented in order to find the cross-sectional warping solutions. The warping solutions obtained contribute the cross-sectional properties to the macroscopic 1D problems. The end effect of the 1D beam problem is also considered via the kinematic correction for a displacement prescribed boundary. The approach presented is applied to the beams with relatively complicated material distributions and cross-sectional geometry. As numerical test-beds, a three-layered sandwich beam and a composite beam with the multi-cell cross-section are taken to analyze the local deformation. A parametric study is also carried out to investigate the significance of shear deformation due to the cross-sectional orthotropic characteristics. The cross-sectional deformation is predicted based on the asymptotic framework. The accuracy of the present approach is assessed by comparing the results obtained with the 3D FEM solutions obtained by ANSYS.

Keywords: Asymptotic expansion method; Cross-sectional analysis; Warping solution; Composite beams

1. Introduction

The composite beam structures have been broadly used in many engineering fields due to their high strength-to-weight properties. The well-developed classical beam theory is applicable to most engineering problems. The classical beam theory is however not valid for the accurate prediction of the mechanical behavior if the sufficient slenderness of beams is not assured. Especially for anisotropic composite beams, it is required to consider the transverse shear deformation effect because the beams are relatively weak in shear. For this reason, many high-order beam theories have been developed. Nevertheless, they still have the limitations in describing the cross-sectional deformation that is important in thin-walled beams and composite sandwich beams. The deformations include non-classical effects such as in-plane warping, out-of-plane warping, and distortion. Such non-classical deformations are of great importance in vibration problems, because the specific modes might be missed [1]. Therefore, it is necessary to carry out the cross-sectional analysis in order to contribute the accurate cross-sectional properties to the macroscopic beam model. For such a purpose, the asymptotic expansion method can serve as the framework of the cross-sectional analysis.

The variational asymptotic method (VAM) was developed by Berdichevsky [2], which applies the asymptotic expansion to the energy functional having one or more small parameters. One of common difficulties in asymptotic expansion methods is boundary conditions especially for displacement prescribed boundaries. To circumvent this, the efforts have been made to derive the Timoshenko-like beam theory based on the VAM [3-5]. The most recent version has been developed by Yu et al. [6], which is built upon the finite element-based cross-sectional analysis. The model based on the VAM and the finite element-based cross-sectional analysis is referred to as VABS (Variational Asymptotic Beam Sectional analysis) since the work of Cesnik and Hodges [4].

In contrast to the VAM, the interior solutions for the formal asymptotic expansion method (FAM) are obtained from the differential equations systematically [7]. However the higher-order effects (e.g. shear deformation) have not been reflected on the beam interior solution. In order to obtain the exact interior solutions, the asymptotically correct boundary conditions should be considered [8]. Buannic and Cartraud [9, 10] proposed the asymptotic model to predict the static behavior of

† This paper was recommended for publication in revised form by Editor Keum Shik Hong

*Corresponding author. Tel.: +82 2 880 1693, Fax.: +82 2 886 1693
E-mail address: mhcho@snu.ac.kr

periodic heterogeneous beams, where the boundary conditions were obtained by employing the decay analysis method [8]. However, it is difficult to obtain these boundary conditions for general engineering applications because of the prior need for the boundary layer state [11, 12]. On the other hands, the simplified boundary conditions were obtained by Horgan and Simmonds [13], and these boundary conditions were applied successfully to the layered orthotropic beams [14]. Recently, a formal asymptotic method-based beam analysis (FAMBA) [15], which is equipped with generalized average boundary conditions for the displacement prescribed boundary, was applied to anisotropic beams with arbitrary cross-sectional geometry, and the results obtained were well correlated to the examples considered therein.

In this paper, the FAMBA is applied to the anisotropic beams with complicated cross-sectional geometry and material distributions. First, we review the asymptotic recursive formulation for slender anisotropic beam structures, in which governing equations and boundary conditions are derived by applying the asymptotic expansion method and employing the virtual work concept at each asymptotic level [15]. A beauty of the asymptotic expansion method is that the method is mathematically rigorous because the primary variables take the forms of power series in terms of the small parameter (i.e. the slenderness of the beam). Although it is verified that the FAMBA is very useful to predict the macroscopic behavior of the beam with the consideration of the suitable boundary conditions at the clamped end, it is needed to investigate if the FAMBA is able to capture the cross-sectional deformation well. In order to assess the capability of the FAMBA further, the cross-sectional analysis is carried out for the cantilever beams with challengeable material distributions and cross-sectional geometry. Under such circumstances, the importance of the edge effect at the clamped end of the beam is examined. To this end, the layered sandwich and the composite beam with the multi-cell cross-section are taken as test-bed examples. The edge effect caused by the clamped boundary is considered and discussed, and the cross-sectional deformation of a composite beam is predicted, which has never been examined before. The accuracy of the presented approach is assessed by comparing the results obtained with the 3D FEM solutions.

2. Recursive asymptotic formulation

A three-dimensional slender beam structure is considered as shown in Fig. 1. For a linear elastic body, the equilibrium equation, the constitutive equation and the strain-displacement relationship are given as follows:

$$\begin{cases} \sigma_{ij,j} + b_i = 0, \\ \sigma_{ij} = C_{ijkl}\varepsilon_{kl}, \\ \varepsilon_{ij} = \left(u_{i,j} + u_{j,i}\right)/2 \end{cases} \tag{1}$$

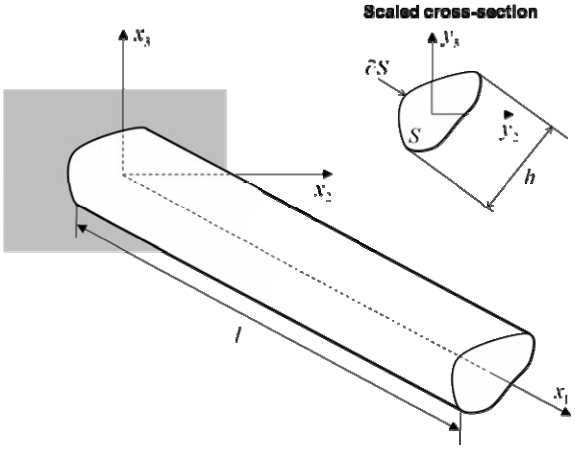

Fig. 1. A three dimensional slender beam.

and the boundary conditions are

$$\begin{cases} \sigma_{ij}n_j^S = t_i^S : \text{prescribed traction at lateral surfaces} \\ \sigma_{ij}n_j = t_i \quad : \text{prescribed traction at } x_1 = 0 \text{ and } x_1 = l_c \\ \mathbf{u} = \bar{\mathbf{u}} \quad : \text{prescribed displacment at } x_1 = 0 \text{ and } x_1 = l_c \end{cases} \tag{2}$$

where n^S and n denote the normal unit vectors to the lateral surface of the beam and to the surface of the beam ends, respectively.

If the small parameter ϵ, which is the ratio of the maximum cross-sectional dimension h and the characteristic length l_c of the beam, is introduced, it is possible to scale the coordinates (x_1, x_2, x_3) as follows:

$$\left(y_1, \quad y_2, \quad y_3\right) = \left(x_1, \quad \frac{x_2}{\epsilon}, \quad \frac{x_3}{\epsilon}\right). \tag{3}$$

Subsequently, plugging Eq. (3) into Eq. (1) yields

$$\begin{cases} \frac{1}{\epsilon}\mathrm{D}_{23}^{\mathrm{T}}\boldsymbol{\sigma} + \mathrm{D}_1^{\mathrm{T}}\boldsymbol{\sigma}_{,1} + \mathbf{b} = 0, \\ \boldsymbol{\sigma} = \frac{1}{\epsilon}\mathbf{C}\mathrm{D}_{23}^{\mathrm{T}}\mathbf{u} + \mathbf{C}\mathrm{D}_1^{\mathrm{T}}\mathbf{u}_{,1}, \\ \mathbf{e} = \frac{1}{\epsilon}\mathrm{D}_{23}\mathbf{u} + \mathrm{D}_1\mathbf{u}_{,1} \end{cases} \tag{4}$$

where the superscript T denotes the transpose of matrices and/or vectors. The displacement, strain, and stress vectors are defined by

$$\begin{aligned} \mathbf{u} &= \left\{u_1 \quad u_2 \quad u_3\right\}^{\mathrm{T}}, \\ \mathbf{e} &= \left\{\varepsilon_{11} \quad \varepsilon_{22} \quad \varepsilon_{33} \quad 2\varepsilon_{23} \quad 2\varepsilon_{13} \quad 2\varepsilon_{12}\right\}^{\mathrm{T}}, \\ \boldsymbol{\sigma} &= \left\{\sigma_{11} \quad \sigma_{22} \quad \sigma_{33} \quad \sigma_{23} \quad \sigma_{13} \quad \sigma_{12}\right\}^{\mathrm{T}} \end{aligned} \tag{5}$$

and the body force vector is $\mathbf{b} = \left\{b_1 \quad b_2 \quad b_3\right\}^{\mathbf{T}}$, and two linear operators D_{23} and D_1 are given as follows:

$$\mathrm{D}_{23}=\begin{bmatrix} 0 & 0 & 0 & 0 & \dfrac{\partial}{\partial y_3} & \dfrac{\partial}{\partial y_2} \\ 0 & \dfrac{\partial}{\partial y_2} & 0 & \dfrac{\partial}{\partial y_3} & 0 & 0 \\ 0 & 0 & \dfrac{\partial}{\partial y_3} & \dfrac{\partial}{\partial y_2} & 0 & 0 \end{bmatrix}^{\mathrm{T}},$$
$$\mathrm{D}_1=\begin{bmatrix} 1 & 0 & 0 & 0 & 0 & 0 \\ 0 & 0 & 0 & 0 & 0 & 1 \\ 0 & 0 & 0 & 0 & 1 & 0 \end{bmatrix}^{\mathrm{T}}. \tag{6}$$

The displacement can be expanded in terms of the small parameter ϵ, and subsequently the strain and stress are asymptotically expanded by substituting the expanded displacement into Eq. (4). These are summarized as follows:

$$\begin{cases} \mathbf{u}(x_i)=\mathbf{u}^0(y_1)+\epsilon\mathbf{u}^1(y_i)+\epsilon^2\mathbf{u}^2(y_i)+\epsilon^3\mathbf{u}^3(y_i)+h.o.t., \\ \mathbf{e}(x_i)=\mathbf{e}^0(y_i)+\epsilon\mathbf{e}^1(y_i)+\epsilon^2\mathbf{e}^2(y_i)+\epsilon^3\mathbf{e}^3(y_i)+h.o.t., \\ \boldsymbol{\sigma}(x_i)=\boldsymbol{\sigma}^0(y_i)+\epsilon\boldsymbol{\sigma}^1(y_i)+\epsilon^2\boldsymbol{\sigma}^2(y_i)+\epsilon^3\boldsymbol{\sigma}^3(y_i)+h.o.t.. \end{cases} \tag{7}$$

The recursive formulation is finally derived by substituting Eq. (7) into Eq. (4), collecting the same order of the small parameter, and scaling the applied tractions and the prescribed displacements [13]. A set of the recursive equations are then given as follows:

$$\begin{cases} \mathrm{D}_{23}^{\mathrm{T}}\boldsymbol{\sigma}^{(k+1)}+\mathrm{D}_1^{\mathrm{T}}\boldsymbol{\sigma}_{,1}^{(k)}+\mathbf{b}^{(k)}=0, \\ \boldsymbol{\sigma}^{(k+1)}=\mathbf{C}\mathbf{e}^{(k+1)}, \qquad k\geq -1 \\ \mathbf{e}^{(k+1)}=\mathrm{D}_{23}\mathbf{u}^{(k+2)}+\mathrm{D}_1\mathbf{u}_{,1}^{(k+1)}, \end{cases} \tag{8}$$

and the associated boundary conditions are

$$\begin{cases} \sigma_{ij}^{(k+1)}n_j^S=t_i^{S(k+1)} & \text{on lateral surfaces of a beam} \\ \sigma_{ij}^{(k+1)}n_j=t_i^{(k+1)} & \text{at } x_1=0 \text{ and } x_1=l_c \\ \mathbf{u}^{(k+1)}=\bar{\mathbf{u}}^{(k+1)} & \text{at } x_1=0 \text{ and } x_1=l_c \end{cases} \tag{9}$$
$$,k\geq -1.$$

In general the analytical solution of Eq. (8) cannot be found, and therefore, a standard finite element discretization is employed to find the warping solutions. Eq. (8) can be split into the two problems; microscopic 2D problems (warping solutions) and macroscopic 1D problems (beam solutions).

3. Microscopic 2D problems

The complete solution at each order k consists of the fundamental solution $\mathbf{u}_f^{(k)}$ and the warping solution $\mathbf{u}_w^{(k)}$.

$$\mathbf{u}^{(k)}=\mathbf{u}_f^{(k)}+\mathbf{u}_w^{(k)} \tag{10}$$

The fundamental solutions represent the rigid-body motions of the cross-section, whereas the warping solutions include the cross-sectional deformation. The warping solutions at each order represent a variety of warping deformations due to the Poisson effect, torsional shear deformation, or transverse shear deformation on the cross-section. The fundamental solution $\mathbf{u}_f^{(k)}$ can be obtained in the mathematical framework, whereas the numerical methods should be employed in order to obtain the warping solution $\mathbf{u}_w^{(k)}$ in general. For the warping solutions, the virtual work concept is introduced to apply a finite element discretization. The variational form of the equilibrium equation in Eq. (8) can be expressed by

$$\int_S \delta\left(\mathrm{D}_{23}\mathbf{u}^{(k+2)}\right)^{\mathrm{T}}\boldsymbol{\sigma}^{(k+1)}dS = \int_S \delta\left(\mathbf{u}^{(k+2)}\right)^{\mathrm{T}}\left(\mathrm{D}_1^{\mathrm{T}}\boldsymbol{\sigma}_{,1}^{(k+1)}+\mathbf{b}^{(k+1)}\right)dS+\int_{\partial S}\delta\left(\mathbf{u}^{(k+2)}\right)^{\mathrm{T}}\mathbf{t}^{S(k+1)}dS,$$
$$k\geq 0, \tag{11}$$

where the terms associated with $\delta\mathbf{u}_w^{(k)}$ form the microscopic 2D problems for the warping solutions to be found.

The first microscopic problem starts from $k=-1$. The complete solution $\mathbf{u}^{(1)}$ is composed of the homogeneous solution $\mathbf{u}_h$ and the particular solution $\mathbf{u}_p$. The homogeneous solution $\mathbf{u}_h$ represents the rigid body motions, which include three translations and a rotation with respect to the reference line. The particular solution corresponds to the solution of the Euler-Bernoulli beam theory such that

$$\mathbf{u}_p^{(1)}=\begin{Bmatrix} -y_3\hat{u}_{3,1}^{(0)}-y_2\hat{u}_{2,1}^{(0)} \\ 0 \\ 0 \end{Bmatrix} \tag{12}$$

which makes the zeroth-order strain vanish.

Consequently the fundamental solutions at each order take the same form of the first-order displacement [9, 15], which are expressed as follows:

$$\mathbf{u}_f^{(k)}(y_i)=\mathbf{u}_h^{(k)}(y_i)+\mathbf{u}_p^{(k)}(y_i)=\mathbf{T}_1\mathbf{v}^{(k)}(y_1) \tag{13}$$

where

$$\mathbf{T}_1=\begin{bmatrix} 1 & 0 & 0 & 0 & -y_2 & -y_3 \\ 0 & 1 & 0 & -y_3 & 0 & 0 \\ 0 & 0 & 1 & y_2 & 0 & 0 \end{bmatrix},$$
$$\tilde{\mathbf{v}}^{(k)}=\left\{\hat{u}_1^{(k)}\ \hat{u}_2^{(k)}\ \hat{u}_3^{(k)}\ \hat{\phi}^{(k)}\right\}^{\mathrm{T}},$$
$$\mathbf{v}^{(k)}=\left\{\tilde{\mathbf{v}}^{\mathrm{T}}\ \hat{u}_{2,1}^{(k-1)}\ \hat{u}_{3,1}^{(k-1)}\right\}^{\mathrm{T}}. \tag{14}$$

Henceforth the variables with a hat (^) in Eq. (14) indicate functions of y_1 only.

The warping solution turns up from the second microscopic problem $(k=0)$. After applying the integration by parts and the divergence theorem to the equilibrium equations for the

microscopic 2D problems, the finite element formulation can be derived by discretizing the warping displacement. For the second microscopic problem, the finite element formulation [15] is given by

$$\mathbf{K}_{23}\,\bar{\mathbf{u}}_w^{(2)} = \mathbf{F}_{23}^{(1)} \tag{15}$$

where the stiffness matrix $\mathbf{K}_{23}$ and the force vector $\mathbf{F}_{23}^{(1)}$ are defined as follows:

$$\begin{aligned}\mathbf{K}_{23} &= \int_S \mathbf{B}_{23}^{\mathrm{T}}\mathbf{C}\mathbf{B}_{23}dS\,\bar{\mathbf{u}}_w^{(2)},\\ \mathbf{F}_{23}^{(1)} &= -\int_S \mathbf{B}_{23}^{\mathrm{T}}\mathbf{C}\mathrm{D}_1\mathbf{u}_{,1}^{(1)}dS = -\int_S \mathbf{B}_{23}^{\mathrm{T}}\mathbf{C}\mathbf{T}_2 dS\,\tilde{\mathbf{v}}_{,1}^{(1)}\end{aligned} \tag{16}$$

in which $\bar{\mathbf{u}}_w$ is the nodal vector, and

$$\mathbf{T}_2 = \begin{bmatrix} 1 & -y_2 & -y_3 & 0 \\ 0 & 0 & 0 & -y_3 \\ 0 & 0 & 0 & y_2 \end{bmatrix}. \tag{17}$$

The strain-displacement matrix is defined by

$$\mathbf{B}_{23} = \mathrm{D}_{23}\mathbf{N}_{23} \tag{18}$$

where $\mathbf{N}_{23}$ denotes the shape function.

The stiffness matrix in Eq. (15) includes four zero-eigenvalues which correspond to the rigid body modes. At this point, the constraints should be enforced to remove those modes by employing the penalty functions [16]. The penalty number is chosen to be the largest eigenvalue of the stiffness matrix. As a result, the warping solution is represented by

$$\mathbf{B}\bar{\mathbf{u}}_w^{(2)} = \boldsymbol{\Psi}^{(1)}\tilde{\mathbf{v}}_{,1}^{(1)} \tag{19}$$

where $\boldsymbol{\Psi}^{(1)}$ is the discretized cross-sectional deformation matrix, which accounts for the three-dimensional Poisson effect on the cross-section.

By following the same procedure described in the above, the third microscopic problem can be formulated. Unlike the second microscopic problem, the body force and lateral surface tractions appear at the problem. The body force $\mathbf{b}^{(k)}$ and lateral surface traction vector $\mathbf{t}^{\mathbf{S}(k+1)}$ are assumed to take the form of

$$\begin{aligned}\mathbf{b}^{(k)}(y_i) &= \bar{\mathbf{b}}^{(k)}(y_2,y_3)\hat{\mathbf{b}}^{(k)}(y_1),\\ \mathbf{t}^{\mathbf{S}(k+1)}(y_i) &= \bar{\mathbf{t}}^{\mathbf{S}(k+1)}(y_2,y_3)\hat{\mathbf{t}}^{\mathbf{S}(k+1)}(y_1).\end{aligned} \tag{20}$$

Thus they can be smeared into the microscopic problems. The finite element formulation is then given by

$$\mathbf{K}_{23}\bar{\mathbf{u}}_w^{(3)} = \mathbf{F}_{23}^{(2)} \tag{21}$$

where

$$\begin{aligned}\mathbf{F}_{23}^{(2)} = &-\int_S \mathbf{B}_{23}^{\mathrm{T}}\mathbf{C}\mathbf{T}_2 dS\,\tilde{\mathbf{v}}_{,1}^{(2)} + \int_S \mathbf{B}_1^{\mathrm{T}}\mathbf{C}\mathbf{T}_2 dS\,\tilde{\mathbf{v}}_{,11}^{(1)}\\ &+\left(\int_S \mathbf{B}_{23}^{\mathrm{T}}\mathbf{C}\mathbf{B}_1 dS - \int_S \mathbf{B}_1^{\mathrm{T}}\mathbf{C}\mathbf{B}_{23}dS\right)\bar{\mathbf{u}}_{w,1}^{(2)}\\ &+\int_S \mathbf{N}_{23}^{\mathrm{T}}\bar{\mathbf{b}}^{(1)}dS\,\hat{\mathbf{b}}^{(1)} + \int_{\partial S}\mathbf{N}_{23}^{\mathrm{T}}\bar{\mathbf{t}}^{\mathbf{S}(2)}dS\,\hat{\mathbf{t}}^{\mathbf{S}(2)}\end{aligned} \tag{22}$$

and

$$\mathbf{B}_1 = \mathrm{D}_1\mathbf{N}_{23}. \tag{23}$$

The third order warping solution is obtained by solving Eq. (21) as follows:

$$\bar{\mathbf{u}}_w^{(3)} = \boldsymbol{\Psi}^{(1)}\tilde{\mathbf{v}}_{,1}^{(2)} + \boldsymbol{\Psi}^{(2)}\tilde{\mathbf{v}}_{,11}^{(1)} + \bar{\mathbf{u}}_{bt^S}^{(3)} \tag{24}$$

where $\bar{\mathbf{u}}_{bt^S}^{(3)}$ is the displacement caused by the body force and the lateral surface traction (i.e. 4th and 5th terms in Eq. (22)), and $\boldsymbol{\Psi}^{(2)}$ includes cross-sectional deformation modes (mainly shear deformation).

For the higher order microscopic 2D problems, the warping solutions are finally generalized as follows [15]:

$$\bar{\mathbf{u}}_w^{(k)} = \sum_m^k \boldsymbol{\Psi}^{(m)}\frac{\partial^{m-1}\tilde{\mathbf{v}}^{(k-m+1)}}{\partial y_1^{m-1}} + \bar{\mathbf{u}}_{bt^S}^{(k)}, \qquad k \geq 4. \tag{25}$$

4. Macroscopic 1D problems

The equilibrium equations of macroscopic 1D problems can be derived from the terms associated with the variation of the fundamental solution $\mathbf{u}_f^{(k)}$ in Eq. (11). The first equilibrium equation appears at $k=0$, and the set of equilibrium equations at each order can be obtained subsequently. The warping solutions obtained from the microscopic 2D problems are systematically smeared into the macroscopic 1D problems. The 1D constitutive equations at each order are constructed from the relationship between the stress resultants and the macroscopic strains.

Finally, the finite element 1D beam formulation can be derived via the weak forms of the macroscopic 1D problems given in Eq. (11). The first order beam equations are then obtained by

$$\mathbf{K}_1\,\mathbf{V}^{(1)} = \mathbf{F}_1^{(1)} \tag{26}$$

where the stiffness matrix $\mathbf{K}_1$ is given by

$$\mathbf{K}_1 = \int_0^{l_e}\mathbf{B}^{(1)\mathrm{T}}\mathbf{E}^{(1)}\mathbf{B}^{(1)}dy_1 \tag{27}$$

in which the strain-displacement matrix is defined as follows:

$$\mathbf{B}^{(m)} = \mathrm{D}^{(m)}\mathbf{N}_1, \tag{28}$$

$$\mathrm{D}^{(m)}=\begin{bmatrix} \dfrac{\partial^m}{\partial {y_1}^m} & 0 & 0 & 0 \\ 0 & \dfrac{\partial^{m+1}}{\partial {y_1}^{m+1}} & 0 & 0 \\ 0 & 0 & \dfrac{\partial^{m+1}}{\partial {y_1}^{m+1}} & 0 \\ 0 & 0 & 0 & \dfrac{\partial^m}{\partial {y_1}^m} \end{bmatrix}, \qquad \mathbf{N}_1=\begin{bmatrix} N_i & 0 & 0 & 0 & 0 & 0 \\ 0 & M_i & 0 & 0 & H_i & 0 \\ 0 & 0 & M_i & 0 & 0 & H_i \\ 0 & 0 & 0 & N_i & 0 & 0 \end{bmatrix}. \tag{29}$$

In Eq. (29), the shape function N_i is the one-dimensional Lagrange polynomial, and the shape functions M_i and H_i are the one-dimensional Hermite polynomial. In Eq. (27), the matrix $\mathbf{E}^{(1)}$ and the force vector are calculated as follows:

$$\begin{aligned}\mathbf{E}^{(1)}&=\int_S \left(\mathrm{D}_1\mathbf{T}_2\right)^{\mathrm{T}}\mathbf{C}\left(\mathrm{D}_1\mathbf{T}_2\right)dS \\ &\quad+\int_S \left(\mathrm{D}_1\mathbf{T}_2\right)^{\mathrm{T}}\mathbf{C}\mathbf{B}_{23}\boldsymbol{\Psi}^1 dS,\end{aligned} \tag{30}$$

$$\mathbf{F}^{(1)}=\int_0^{l_c}\mathbf{N}_1{}^{\mathrm{T}}\tilde{f}_b^{(1)}dy_1+\int_0^{l_c}\mathbf{N}_1{}^{\mathrm{T}}\left(\tilde{f}^{(1)}+\tilde{f}^{(2)}\right)dy_1 \tag{31}$$

where the forcing terms $\tilde{f}_b^{(1)}$ and $\tilde{f}^{(k)}$ are defined by

$$\begin{aligned}\tilde{f}_b^{(1)}&=\begin{Bmatrix} r_1 & r_2 & r_3 & 0 & r_{m2} & r_{m3}\end{Bmatrix}^{\mathrm{T}}, \\ \tilde{f}^{(1)}&=\begin{Bmatrix} f_1 & 0 & 0 & 0 & m_2 & m_3\end{Bmatrix}^{\mathrm{T}}, \\ \tilde{f}^{(2)}&=\begin{Bmatrix} 0 & f_2 & f_3 & 0 & 0 & 0\end{Bmatrix}^{\mathrm{T}},\end{aligned} \tag{32}$$

in which

$$\begin{aligned}r_1&=\int_S \bar{\mathbf{b}}_1^{(1)}dS\hat{\mathbf{b}}_1^{(1)}+\int_{\partial S}\bar{\mathbf{t}}_1^{\mathbf{S}(2)}dS\hat{\mathbf{t}}_1^{\mathbf{S}(2)}, \\ r_\alpha&=\int_S \bar{\mathbf{b}}_\alpha^{(2)}dS\hat{\mathbf{b}}_\alpha^{(2)}+\int_{\partial S}\bar{\mathbf{t}}_\alpha^{\mathbf{S}(3)}dS\hat{\mathbf{t}}_\alpha^{\mathbf{S}(3)}, \\ r_{m\alpha}&=\int_S y_\alpha\bar{\mathbf{b}}_1^{(1)}dS\hat{\mathbf{b}}_1^{(1)}+\int_{\partial S}y_\alpha\bar{\mathbf{t}}_1^{\mathbf{S}(2)}dS\hat{\mathbf{t}}_1^{\mathbf{S}(2)}, \\ f_i&=\int_S \mathbf{t}_i dS,\ m_\alpha=\int_S y_\alpha\mathbf{t}_i dS\end{aligned} \qquad (\alpha=2,3). \tag{33}$$

By following the procedure described in the above, the second order macroscopic 1D problem is summarized by

$$\mathbf{K}_1\mathbf{V}^{(2)}=\mathbf{F}_1^{(2)}+\mathbf{F}_{1f}^{(2)} \tag{34}$$

where the force vector $\mathbf{F}_1^{(2)}$ now includes the applied torque, and the force vector $\mathbf{F}_{1f}^{(2)}$ does the higher-order effects. These vectors are given by

$$\begin{aligned}\mathbf{F}_1^{(2)}&=\int_0^{l_c}\mathbf{N}_1{}^{\mathrm{T}}\tilde{f}_b^{(2)}dy_1+\int_0^{l_c}\mathbf{N}_1{}^{\mathrm{T}}\tilde{f}_\tau^{(2)}dy_1, \\ \mathbf{F}_f^{(2)}&=\int_0^{l_c}\mathbf{B}^{(1)\mathrm{T}}\mathbf{E}^{(2)}\mathbf{B}^{(2)}\mathbf{v}^{(1)}dy_1 \\ &\quad+\int_0^{l_c}\left(\mathrm{D}_1\mathbf{T}_2\right)^{\mathrm{T}}\mathbf{C}\mathbf{B}_{23}\bar{\mathbf{u}}_{bt^s}^{(3)}dy_1\end{aligned} \tag{35}$$

where

$$\begin{aligned}\tilde{f}_b^{(2)}&=\begin{Bmatrix}0 & 0 & 0 & r_4 & 0 & 0\end{Bmatrix}^{\mathrm{T}}, \\ \tilde{f}_\tau^{(2)}&=\begin{Bmatrix}0 & 0 & 0 & \tau & 0 & 0\end{Bmatrix}^{\mathrm{T}},\end{aligned} \tag{36}$$

$$\begin{aligned}r_4&=\int_S y_2\bar{\mathbf{b}}_3^{(2)}\hat{\mathbf{b}}_3^{(2)}-y_3\bar{\mathbf{b}}_2^{(2)}\hat{\mathbf{b}}_2^{(2)}dS \\ &\quad+\int_{\partial S}y_2\bar{\mathbf{t}}_3^{\mathbf{S}(3)}\hat{\mathbf{t}}_3^{\mathbf{S}(3)}-y_3\bar{\mathbf{t}}_2^{\mathbf{S}(3)}\hat{\mathbf{t}}_2^{\mathbf{S}(3)}dS,\end{aligned} \tag{37}$$

$$\begin{aligned}\tau&=\int_S y_2\mathbf{t}_3-y_3\mathbf{t}_2dS, \\ \mathbf{E}^{(k)}&=\int_S\left(\mathrm{D}_1\mathbf{T}_2\right)^{\mathrm{T}}\mathbf{C}\mathbf{B}_1\boldsymbol{\Psi}^{(k-1)}dS \\ &\quad+\int_S\left(\mathrm{D}_1\mathbf{T}_2\right)^{\mathrm{T}}\mathbf{C}\mathbf{B}_{23}\boldsymbol{\Psi}^{(k)}dS.\end{aligned} \tag{38}$$

The third order macroscopic 1D problem is given by

$$\mathbf{K}_1\mathbf{V}^{(3)}=\mathbf{F}_1^{(3)}+\mathbf{F}_{1f}^{(3)} \tag{39}$$

where

$$\begin{aligned}\mathbf{F}_1^{(3)}&=0, \\ \mathbf{F}_{1f}^{(3)}&=\int_0^{l_c}\mathbf{B}^{(1)\mathrm{T}}\mathbf{E}^{(2)}\mathbf{B}^{(2)}dy_1\mathbf{v}^{(2)}+\int_0^{l_c}\mathbf{B}^{(1)\mathrm{T}}\mathbf{E}^{(2)}\mathbf{B}^{(3)}dy_1\mathbf{v}^{(1)} \\ &\quad+\int_0^{l_c}\left(\mathrm{D}_1\mathbf{T}_2\right)^{\mathrm{T}}\mathbf{C}\mathbf{B}_{23}\bar{\mathbf{u}}_{bt^s}^{(4)}dy_1.\end{aligned} \tag{40}$$

Finally, the higher-order macroscopic 1D beam equations can be now generalized as follows:

$$\mathbf{K}_1\mathbf{V}^{(k)}=\mathbf{F}_{1f}^{(k)}, \tag{41}$$

where $\mathbf{V}^{(k)}=\begin{Bmatrix}\hat{u}_1^{(k)} & \hat{u}_2^{(k-1)} & \hat{u}_3^{(k-1)} & \hat{\phi}^{(k)} & \hat{u}_{2,1}^{(k-1)} & \hat{u}_{3,1}^{(k-1)}\end{Bmatrix}$, and

$$\begin{aligned}\mathbf{F}_{1f}^{(k)}&=\sum_{m=2}^{k}\int_0^{l_c}\mathbf{B}^{(1)\mathrm{T}}\mathbf{E}^{(m)}\mathbf{B}^{(m)}dy_1\mathbf{v}^{(k-m+1)} \\ &\quad+\int_0^{l_c}\left(\mathrm{D}_1\mathbf{T}_2\right)^{\mathrm{T}}\mathbf{C}\mathbf{B}_{23}\bar{\mathbf{u}}_{bt^s}^{(k)}dy_1, \qquad k\geq 4.\end{aligned} \tag{42}$$

5. Results and discussion

In this section, the cross-sectional deformations are examined by substituting the solutions of the macroscopic 1D problems $\mathbf{V}^{(k)}$ into the microscopic 2D problems. The solutions of the macroscopic 1D problems are expanded up to the third-order because the higher order solutions are relatively negligible. In order to calculate the third order solutions, one needs to calculate the higher order derivatives with respect to the reference coordinate. To this end, the quadratic interpolation functions and the fifth-order Hermite interpolation functions are

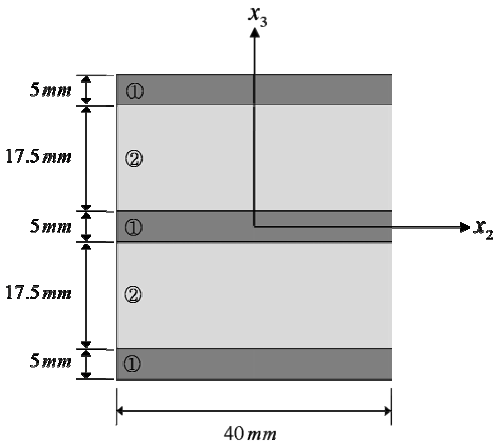

Fig. 2. The configuration of the cross-section of a layered beam.

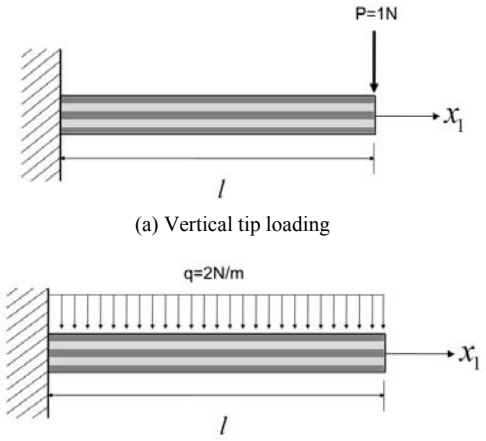

(a) Vertical tip loading

(b) Distributed loading

Fig. 3. Loading conditions.

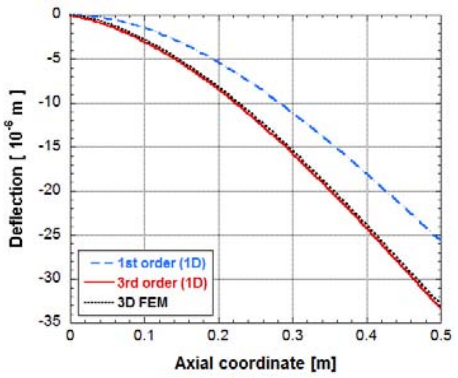

(a) Vertical tip loading

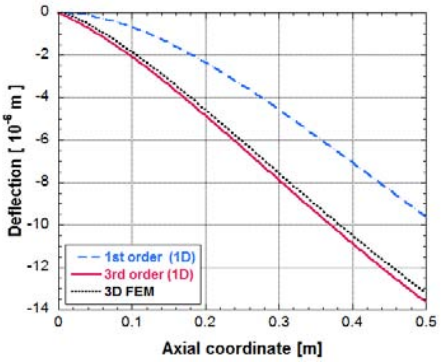

(b) Distributed loading

Fig. 4. Deflection curves of a layered beam.

employed for C^0 variables and C^1 variables, respectively. For the finite element discretization of the microscopic 2D problems, the four-noded quadrilateral QM6 element [17] is employed, in which the incompatible modes are added to remedy the membrane-locking defect caused by Q4 element. As illustrative examples, a three-layered sandwich beam with rectangular cross-sectional geometry and a composite beam with the multi-cell cross-section where the beam boundary conditions are fixed and free (i.e. a cantilever). In the asymptotic approaches, the displacement prescribed boundary is generally problematic [10]. In this study, the averaged boundary conditions for the clamped boundary are used to provide the appropriate boundary conditions for the proposed asymptotic model, which can be found in the Ref. [15]. In all reported figures, the three-dimensional FEM solutions, where the 8 noded-hexahedral element is used, are taken as the reference solutions, which are calculated by using the commercial software ANSYS [18].

5.1 A layered sandwich beam with rectangular cross–sectional geometry

A configuration of the layered sandwich beam is shown in Fig. 2, and the mechanical properties of each layer are $E_1 = 80$ GPa, $E_2 = 0.8$ GPa, $v_1 = 0.33$ and $v_2 = 0.4$, respectively. As shown in Fig. 3, cantilevered layered sandwich beams under the vertical tip loading and the distributed loading are analyzed, where the length of the beam is 0.5 m. The first order solution $\mathbf{V}^{(1)}$ of the macroscopic 1D problem corresponds to the classical Euler-Bernoulli beam theory, and the second order solution $\mathbf{V}^{(2)}$ vanishes for these loading conditions because there is no shear-torsion coupling. The third order solution $\mathbf{V}^{(3)}$ includes the shear deformation effect via the non-zero slope boundary condition at the clamped end, which incorporates the edge effect into the solution [15].

For the two loading cases, the deflection along the axial coordinate is plotted in Figs. 4(a) and (b), where the first and third order solutions are compared to the 3D FEM results. For the 3D FEM analysis, 32000 solid elements are used, and the displacements at the centroid of the cross-section of the beam are extracted along the axial coordinate. As shown in Figs. 4(a) and (b), the classical beam theory (i.e. the first order solution) shows a large deviation from the 3D FEM, whereas the third order solution, which considers the kinematically corrected boundary condition at the clamped end, provides the reliable result. The edge effects caused by the clamped end have significant influence on the deflection of a composite beam. Thus, the appropriate boundary conditions at the

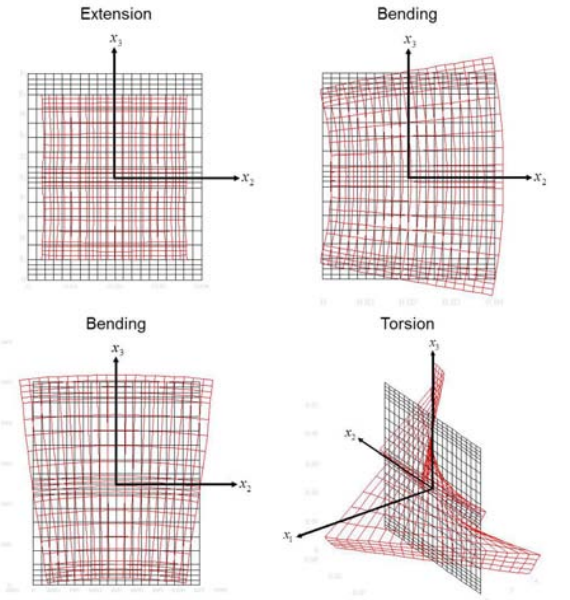

Fig. 5. The first-order cross-sectional deformation mode $\mathbf{\Psi}^{(1)}$ of a layered beam.

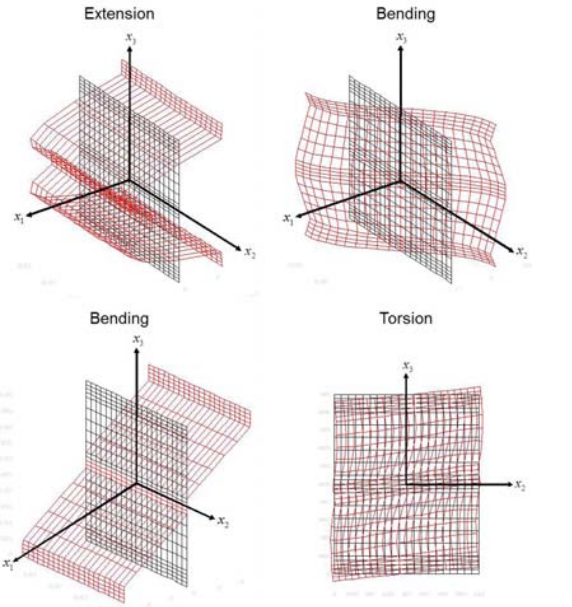

Fig. 6. The second-order cross-sectional deformation mode $\mathbf{\Psi}^{(2)}$ of a layered beam.

clamped end should be taken into consideration as mentioned previously. It is revalidated that the simplified asymptotically correct boundary conditions at a clamped end [15] are available to the general cantilever composite beams.

The first order and second order deformation modes are illustrated in Figs. 5 and 6, where one can see that deformed shapes of the cross-section of the beams are easily visible and/or predictable via the matrix $\mathbf{\Psi}$. In Fig. 5, the deformation mode $\mathbf{\Psi}^{(1)}$, which comes from the second microscopic 2D problem, includes the cross-sectional deformations due to the Poisson effects and the Saint-Venant torsion. One can

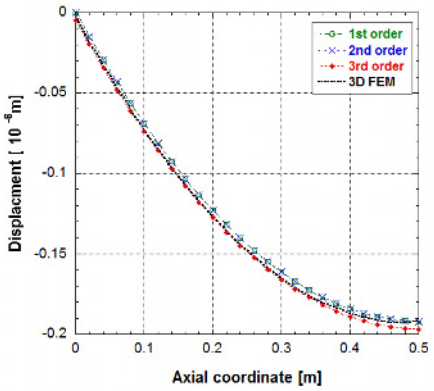

(a) x_1 direction

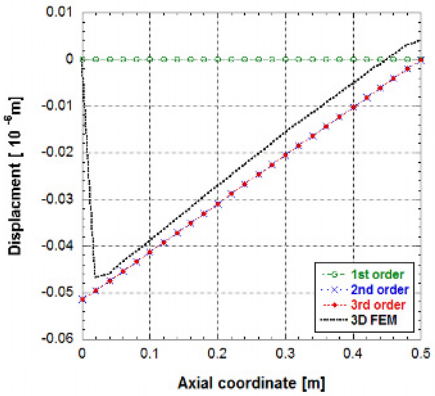

(b) x_2 direction

Fig. 7. Displacement solutions for a vertical tip loading along the axial coordinate.

clearly see that the torsional warping is quite complicate for this example, unlike simple rectangular cross-section case. This kind of warping is almost impossible to presuppose, which justifies why one has to consider the asymptotic approach proposed. In Fig. 6, the deformation mode $\mathbf{\Psi}^{(2)}$ from the third microscopic 2D problem accounts for the out-of-plane warping due to tension and shear deformations and the in-plane distortion due to torsion. The well-known zigzag warping for the bending of layered composite beams is captured very well, which is induced by the shear deformation.

In order to demonstrate the capability of predicting the three-dimensional displacements by the approach proposed, the displacements at the left corner on the bottom of the cross-section (see Fig. 2) along the axial coordinate are examined. In Figs. 7(a) and (b), the in-plane and out-of-plane displacements of the beam under the vertical tip loading are plotted and compared to the 3D FEM. In Figs. 8(a) and (b), the displacements for the beam under the distributed loading are also plotted. Figs. 7(b) and 8(b) show the three-dimensional Poisson effects due to the beam bending, where it can be clearly seen that the second order solution $\mathbf{u}^{(2)}$ recovers the in-plane warping deformation. The solution is comparable to the 3D FEM prediction. On the other hand, the third order solution $\mathbf{u}^{(3)}$ reflects the out-of-plane warping due to the shear defor-

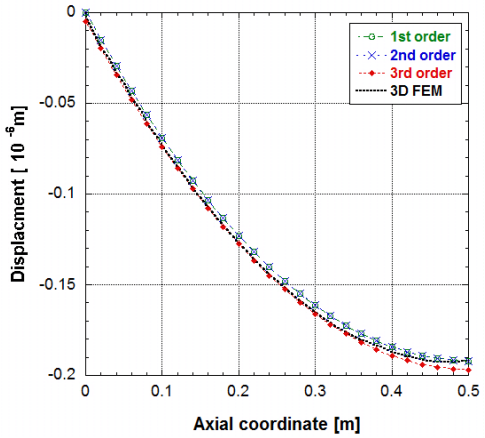

(a) x_1 direction

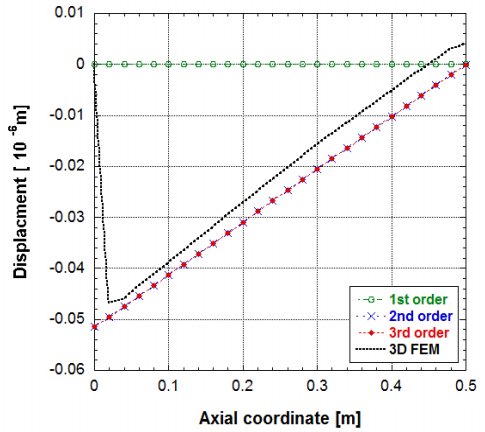

(b) x_2 direction

Fig. 8. Displacement solutions on the cross-section for a distributed loading along the axial coordinate.

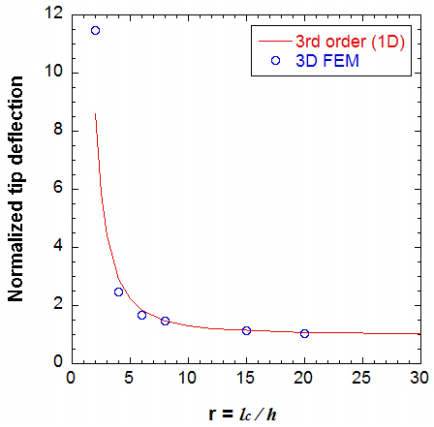

(a) Under the vertical tip loading

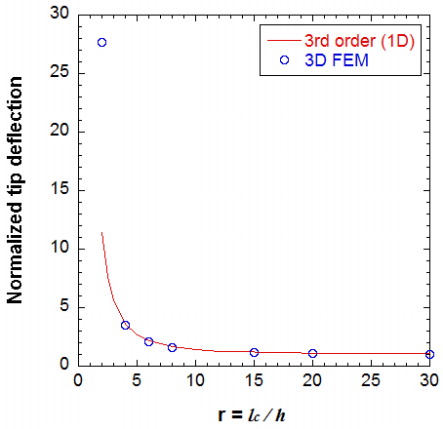

(b) Under the distributed loading

Fig. 9. Normalized tip deflection of a layered beam vs. the length-to-thickness ratio.

mation of the beam cross-section, as shown in Figs. 7(a) and 8(a). The results obtained by the present approach are correlated very well with the 3D FEM in the interior zone, whereas they deviate from the 3D FEM in the edge zones. The averaged boundary conditions employed in this study do not correct the edge zone solutions (or the boundary layer solutions) but the interior solutions. This clearly demonstrates that the asymptotically correct boundary conditions may differ from the physical boundary conditions for the displacement prescribed boundaries to accurately predict the exact interior state.

In general, the classical beam theory is valid only if the cross-sectional dimension is small enough as compared to the beam axial dimension (i.e. the slenderness of the beam should be assured). Otherwise, the deflections obtained by the classical beam theory will significantly deviate from the 3D FEM results. In other words, the edge effect does not decay even far from the edge of the beam weak in shear (i.e. when the beam is not slender in terms of the geometric dimension or the wave length). To investigate the convergence of the present approach, the third order tip deflections of the beam with varying the thickness ratio under the two loading conditions are plotted in Fig. 9, where they are normalized by the first order solution. It is again seen that the third order solutions show an excellent agreement with the 3D FEM results irrespective of the slenderness of the beams.

To demonstrate further the usefulness of the present approach, the orthotropic significance is also investigated. The beam cross-sectional geometry is the same as the previous example, while the material properties are varied. The Young's modulus of E_2 varies whereas E_1 is fixed as 200 GPa and $\nu_1 = \nu_2 = 0.3$. For the beam subjected to the vertical tip loading, the interior solutions at the middle of a beam with varying the ratio (E_1 / E_2) are illustrated in Fig. 10 in which displacements are obtained at the left corner on the bottom of the cross-section. When E_1 / E_2 is 1, it indicates the isotropy of the cross-section, and an increase of the ratio of E_1 / E_2 can be appreciated as the stronger orthotropy of the cross-section. For the isotropy case of the cross-section, the third order solution does not display a remarkable deviation as compared to the first order solution (i.e. classical beam theory). However, the classical beam theory shows a significant deviation from the 3D FEM, as the orthotropy of the cross-section

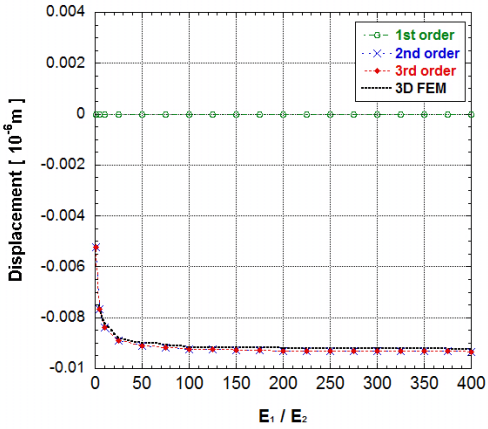

(a) x_2 direction

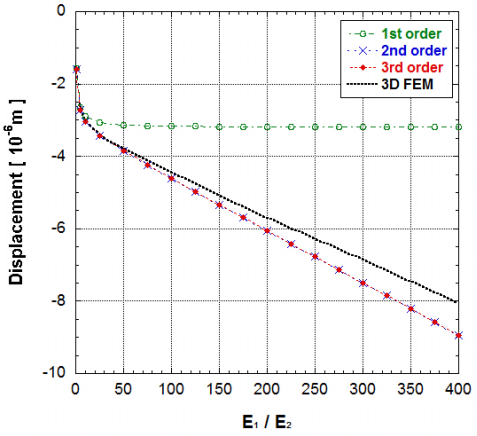

(b) x_3 direction

Fig. 10. The displacement solutions at the left-bottom corner on the cross-section and the beam mid-span with varying the ratio of E_1/E_2.

(i.e., the ratio of E_1/E_2) increases. As shown in Fig. 10(a), the warping displacement due to the Poisson effect increases sharply and is converged soon as the orthotropy of the cross-section become stronger. While the present approach describes this warping displacement very well, for the displacement in the x_3 direction, the deviation from 3D FEM grows as the ratio of E_1/E_2 increases. It can be understood that the significance of the edge effect is strongly affected by the cross-section material distributions. Except the case of drastic orthotropy of the cross-section, the third order solution obtained by applying the generalized average boundary conditions agrees well with the 3D FEM. From this investigation, it is confirmed that the significance of the edge effect is strongly affected by the cross-section material distributions as well as the geometric slenderness of the beam.

5.2 A Composite beam with the multi-cell cross-section

In order to demonstrate the capability of the present asymptotic beam analysis, the composite beam with a multi-cell cross-section is considered as a representative numerical example.

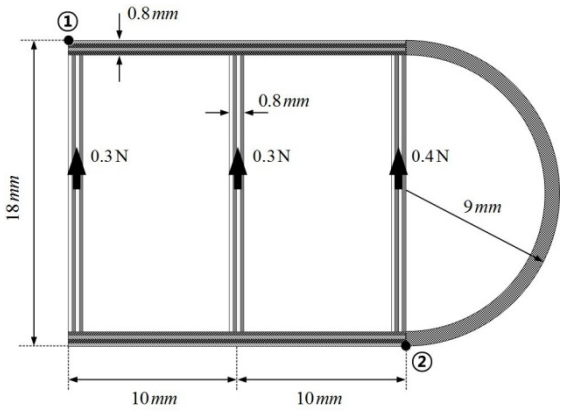

Fig. 11. Geometry of the composite beam with the multi-cell cross-section and loading conditions.

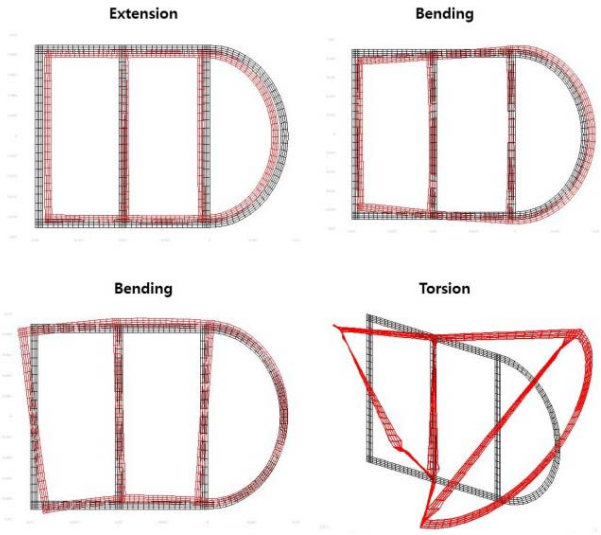

Fig. 12. The first-order cross-sectional deformation mode $\Psi^{(1)}$ of a composite beam with the multi-cell cross section.

The configuration of the multi-cell cross-section is shown in Fig. 11. The material properties in layups and a D shape are

- layups part

$E_{11}=172.4$ GPa, $E_{22}=E_{33}=6.9$ GPa,
$G_{12}=G_{13}=3.45$ GPa, $G_{23}=1.38$ GPa,
$\nu_{12}=\nu_{23}=\nu_{13}=0.25$.

- D shape part

$E_{11}=177$ GPa, $E_{22}=E_{33}=10.8$ GPa,
$G_{12}=G_{13}=7.6$ GPa, $G_{23}=8.5$ GPa,
$\nu_{12}=\nu_{23}=\nu_{13}=0.27$

and upper and lower walls have an angle ply $[15/-15]_2$, and the layups for vertical walls is a cross ply $[0/90]_2$. The equivalent loadings correspond to $r_3=1$ and $\tau=-2.6385\times10^{-3}$ in Eqs. (32) and (36).

The cross sectional deformed shape in a complicated composite beam are observable very easily via the microscopic 2D analysis, the first order deformation modes $\Psi^{(1)}$ are represented in Fig. 12, where 736 QM6 elements [17] are used for

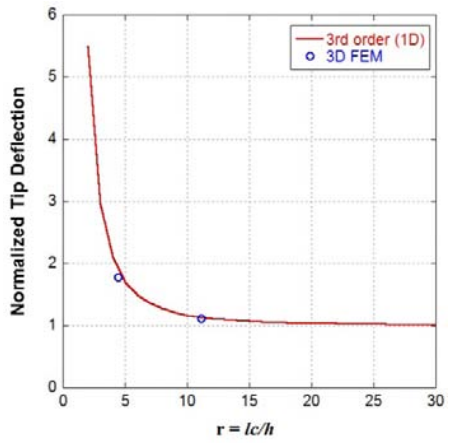

Fig. 13. Normalized tip deflection of a composite beam with the multi-cell cross-section vs. the length-to-thickness ratio.

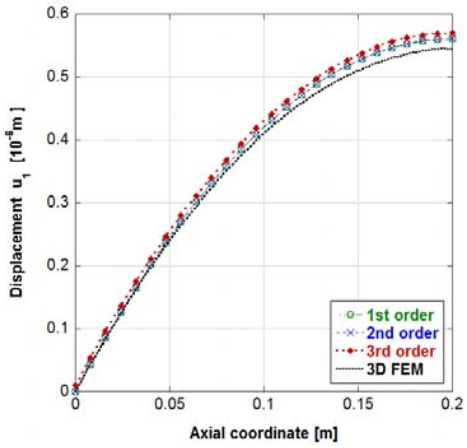

(a) At ① position

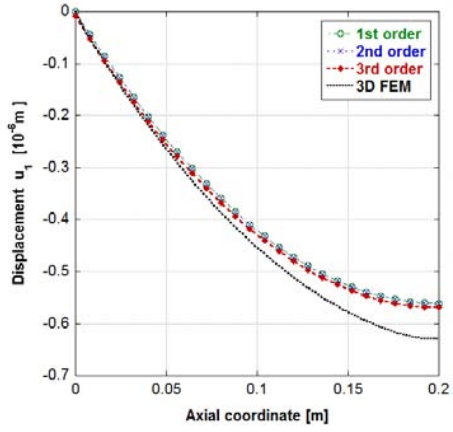

(b) At ② position

Fig. 14. Displacement solutions $\mathbf{u}_1$ on the cross-section for vertical tip loading and torque.

the two dimensional cross- sectional analysis. To compare the beam solution based on asymptotical framework with the 3D FEM solution, 96960 solid elements are used in the 3D FE analysis. The tip deflection for a unit vertical tip loading with

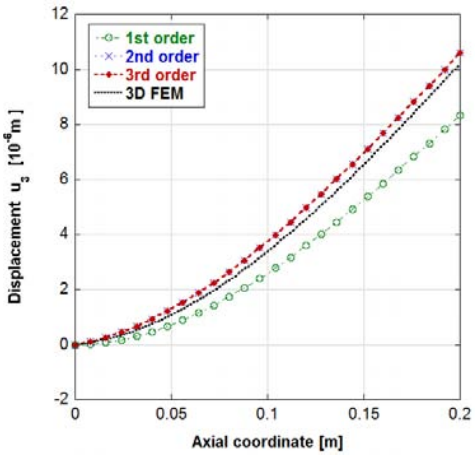

(a) At ① position

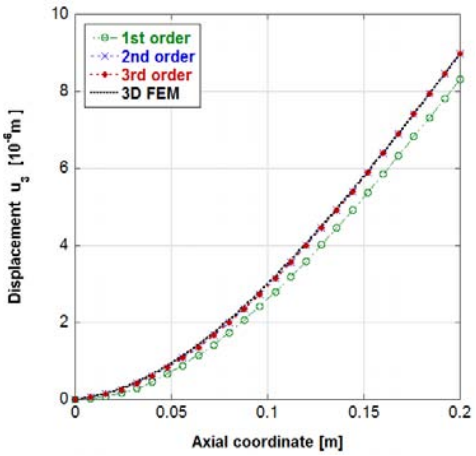

(b) At ② position

Fig. 15. Displacement solutions $\mathbf{u}_3$ on the cross-section for vertical tip loading and torque.

varying the length of a composite beam is examined. The tip deflection is also normalized by the first order beam solution $\mathbf{V}^{(1)}$, and the third order beam solution $\mathbf{V}^{(3)}$ matches the 3D FEM solutions very well as shown in Fig. 13.

The asymmetric configuration due to the cross-sectional geometry and layups induce extension-bending and shear-torsion couplings. Substituting the beam solution $\mathbf{V}^{(k)}$ into Eqs. (12) and (13) makes it possible to capture the complicated cross-sectional deformation with the coupling effect. The displacements are examined at two positions as shown in Fig. 13. Figs. 14 and 15 show the displacement $\mathbf{u}_1$ and $\mathbf{u}_3$, respectively, along the axial coordinate. Because the local deformation caused by the localized point loadings remains, the displacement $\mathbf{u}_1$ on the cross section deviates from the 3D FEM but is still comparable. The displacements solution $\mathbf{u}_3$ based on the asymptotic framework provides very accurate solutions. Especially, the displacement $\mathbf{u}_3$ at position 2 agrees very well with the 3D FEM solutions as shown in Fig. 15(b), since the non-classical deformations on the cross-section are incorporated. In this case, the displacement $\mathbf{u}_2$ is

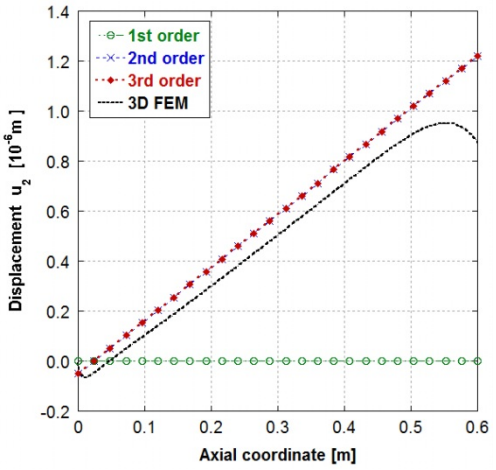

Fig. 16. Displacement solutions $\mathbf{u}_2$ on the cross-section for vertical tip loading and torque at ① position.

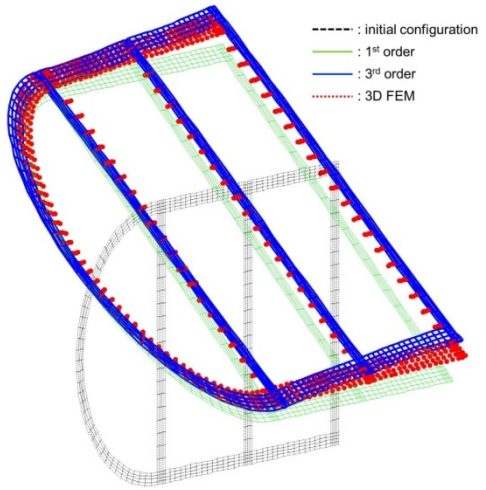

Fig. 17. Cross-sectional deformation at the middle of the beam (beam length : 0.2 m).

dominant due to the torsion and distortion. It is very difficult to capture the local distorted deformation at the free end of a beam due to the highly localized point loadings (i.e., three-dimensional in nature). The displacement $\mathbf{u}_2$ along the axial coordinate is plotted in Fig. 16 when the length of the beam is 0.6 m. The third order solution includes the bending-torsion coupling effect. For a shorter beam (0.2 m-long beam), the cross-sectional deformed shape at the middle of the beam is illustrated in Fig. 17. It can be seen that the third order solution captures well the three-dimensional cross-sectional deformation.

6. Conclusions

The cross-sectional analysis of the beams using an asymptotic expansion method is applied to the layered sandwich beams and the composite beam with the multi-cell cross- section. The asymptotic method with the average boundary conditions for the displacement prescribed boundary is systematically presented to derive the macroscopic 1D and microscopic 2D problems. The warping solutions are obtained by numerically solving the microscopic problems, and then the beam analysis is carried out for the cantilever beams under the vertical tip loading and distributed loading conditions. The deflection obtained by applying the average boundary conditions for the displacement prescribed boundary yields the accurate results as compared to the reference solution (i.e. 3D FEM). The most significant improvement is made by the non-zero slope boundary condition at the clamped end in the third order solution.

The first test-bed example shows that the edge effect is of great importance when the orthotropy of the cross-section is strong. Therefore, the second example, in which the anisotropy is much stronger than the first example because of the complicated material distribution, is presented in order to emphasize the edge effect. The interior solutions obtained are still comparable to the 3D FEM in spite of highly localized point loadings, strong material anisotropy, and complicate geometry.

The main advantage of the beam analysis based on the asymptotic finite element framework is that it can be applied to the beams with complex cross-sectional geometry or material distributions. In addition, the method proposed does not need to calculate the shear correction factors unlike the traditional Rankine-Timoshenko beam theory. Without knowing such the factors, the present approach is able to predict accurately the three-dimensional interior behavior of the beams with challengeable cross-sectional material distribution and geometry. In the computational point of views, it is very efficient as compared to the 3D FEM since it just requires the two-dimensional (cross-sectional) and one-dimensional (beam) discretizations.

Acknowledgment

This work was supported by WCU(World Class University) program through the National Research Foundation of Korea funded by the Ministry of Education, Science and Technology(R31-2010-000-10083-0) and Basic Science Research Program through the National Research Foundation of Korea(NRF) funded by the Ministry of Education, Science and Technology(2011-0014847).

References

[1] J.-S. Kim and K. W. Wang, Vibration analysis of composite beams with end effects via the formal asymptotic method, ASME: Journal of Vibration and Acoustics, 132 (2010) 041003:1-8.

[2] V. L. Berdichevsky, On the energy of an elastic rod, *Journal of Applied Mathematics and Mechanics (PMM)*, 45 (4) (1981) 518-529.

[3] C. E. S. Cesnik, V. G. Sutyrin and D. H. Hodges, Refined

theory of composite beams : the role of short-wavelength extrapolation, *International Journal of Solids and Structures*, 33 (10) (1996) 1387-1408.

[4] C. E. S. Cesnik, V. G. Sutyrin and D. H. Hodges, VABS: a new concept for composite rotor blade cross-sectional modeling, *Journal of American Helicopter Society*, 42 (1) (1997) 27-38.

[5] B. Popescu and D. H. Hodges, On asymptotically correct Timoshenko-like anisotropic beam theory, *International Journal of Solids and Structures*, 37 (2000) 535-558.

[6] W. Yu, D. H. Hodges, V. V. Volovoi and C. E. S. Cesnik, On Timoshenko-like modeling of initially curved and twisted composite beams, *International Journal of Solids and Structures* 39 (2002) 5101-5121.

[7] L. Trabucho and J. M. Viano, Mathematical modeling of rods. In: Ciarlet PG, Lions JL. Handbook of Numerical Analysis, North-Holland (1996) Vol. 4.

[8] R. D. Gregory and F. Y. M. Wan, Decaying states of plane strain in a semi-infinite strip and boundary conditions for plate theory, *Journal of Elasticity*, 14 (1984) 27-64.

[9] N. Buannic and P. Cartraud, Higher-order effective modeling of periodic heterogeneous beams. I. Asymptotic expansion method, *International Journal of Solids and Structures*, 38 (2001a) 7139-7161.

[10] N. Buannic, P. Cartraud, Higher-order effective modeling of periodic heterogeneous beams. II. Derivation of the proper boundary conditions for the interior asymptotic solution, *International Journal of Solids and Structures*, 38 (2001b) 7168-7180.`

[11] H. Fan and G. E. O. Widera, On the proper boundary conditions for a beam, *Journal of Applied Mechanics*, 59 (1992) 915-922.

[12] H. Fan and G. E. O. Widera, On use of variational principles to derive beam boundary conditions, *Journal of Applied Mechanics*, 61 (1992) 470-471.

[13] C. O. Horgan and J. G. Simmonds, Asymptotoic analysis of an end-loaded transversely isotropic, elastic, semi-infinite strip weak in shear, *International Journal of Solids and Structures*, 27 (1991) 1895-1914.

[14] J. M. Duva and J. G. Simmonds, The usefulness of elementary theory for the linear vibrations of layered, orthotropic elastic beams and corrections due to two-dimensional end effect, *Journal of Applied Mechanics*, 58 (1991) 175-180.

[15] J.-S. Kim, M. Cho and E. C. Edward, An asymptotic analysis of composite beams with kinematically corrected end effects, *International Journal of Solids and Structures*, 45 (2008) 1954-1977.

[16] M. Peters and K. Hackl, Numerical aspects of the eXtended finite element method, *Proceeding in Applied Mathematics and Mechanics* , 5 (2005), 355-356.

[17] R. L. Taylor, P. J. Beresford and E. L. Wilson, A nonconforming element for stress analysis, *International Journal for Numerical Methods in Engineering*, 10 (1976) 1211-1219.

[18] ANSYS, ANSYS user's guide release 9.0, 2004.

Joonho Jeong received the B.S. degree from Chungang University, Korea in 2005, and the M.S. degree from Seoul National University, Korea in 2007. He is currently Ph.D candidate in Seoul National University, Korea. His research interests include solid mechanics, structural vibration and multiscale mechanics.

Jun-Sik Kim received the B.S. and M.S. degrees from Inha University, Korea in 1994 and 1996, respectively, and the Ph.D. degree from the Pennsylvania State University, USA in 2005, all in aerospace engineering. In 2009, he joined Kumoh National Institute of Technology, Korea, where he is currently an assistant professor in the department of intelligent mechanical engineering. His research interests include solid mechanics, smart structures, helicopter dynamics, and numerical methods.

Yeon June Kang received his B.S. and M.S. degrees in Mechanical Design and Production Engineering from Seoul National University in 1988 and 1990, respectively. He then went on to receive a Ph.D. degree in Acoustics and Vibration from School of Mechanical Engineering, Purdue University in 1994. After his Ph.D., he continued to work as a Postdoctoral Research until 1996. Since 1997, Dr. Kang is working at the Department of Mechanical and Aerospace Engineering, Seoul National University. Dr. Kang's research interests are in the area of acoustical materials, noise and vibration in automotive engineering and Korean Bells.

Maenghyo Cho received the B.S. and M.S. degree from Seoul National University, Korea in 1984 and 1986, respectively, and Ph.D degree from University of Washington, Seattle, USA in 1993. In 1999, he joined Seoul National University, where he is currently a professor in school of Mechanical and Aerospace Engineering. His research interests include multiscale mechanics, Molecular dynamics, Solid/Structural Mechanics, and Computational Mechanics.